MAGNETIC COUPLING ANALYSIS OF A TET POWER DELIVERY SYSTEM

Thushari Dissanayake, David Budgett
Bioengineering Institute,University of Auckland, 70 Symond Street, Auckland, New Zealand
t.dissanayake@auckland.ac.nz, d.budgett@telemetryresearch.com

Aiguo Patrick Hu
Department of Electrical and Computer Engineering,University of Auckland, 3 Grafton Road, Auckland, New Zealand
a.hu@auckland.ac.nz

Keywords: TET, inductive power transfer, power efficiency, coupling coefficient, mutual inductance.

Abstract: This paper presents a comparative study of methods to determine the coupling coefficient between primary and secondary coils used in a transcutaneous energy transfer system designed for powering implantable biomedical devices. A coupling analysis covering typical misalignments between coils is presented using an analytical model, a simulated model and practical experimental measurements. The simulated model shows good agreement with the experimental measurements. The performance of the system is characterised by carrying out a loss analysis to compute the power efficiency of the system for different misalignment situations. It was established that variable coupling affects the maximum power transfer capacity but has a low impact on the power efficiency for coil separations of less than 30mm.

1 INTRODUCTION

Many implantable biomedical devices require electrical energy for operation. Two common methods of supplying power are using an implantable battery or by having a percutaneous lead from the implant to an external power supply (N. de N. Donaldson 1983). The downsides of these methods are the limited life span of the battery and the potential risk of infection associated with wires through the skin. Inductively coupled power transfer (ICPT) technology enables transfer of power across the skin without direct electrical connectivity. This form of transcutaneous energy transfer (TET) is illustrated in figure 1. The primary coil is located outside the body and generates an electromagnetic field. This time varying field penetrates the skin and induces currents and voltages in the implanted secondary coil which can be used to derive power for the biomedical device.

In high power applications such as left ventricular assist devices (LVADs), the TET coils are located in areas of soft tissue where the coupling conditions are highly variable. Normal patient posture changes or differences in fitting the external parts relative to the internal parts are likely to result in changes to the alignment of the primary and the secondary coils and their relative coupling (John C. Schuder 1971). The coupling between two coils can be represented by their mutual inductance. The definition of mutual inductance is given by Neumann's double integral formula

$$M_{ij} = \frac{\mu_o}{4\pi} \oint\oint \frac{ds_i \cdot ds_j}{R_{ij}} \tag{1}$$

Where μ_o is the permeability of free space, ds_i and ds_j are elements of two coils and R_{ij} is the magnitude of the distance from ds_i to ds_j. This demonstrates that the mutual inductance is a function of the coil geometries and the distance between them (F.C Flack 1971). A more intuitive representation of coil coupling is given by the coupling coefficient, k, defined by:

$$k = \frac{M}{\sqrt{L_1 L_2}} \tag{2}$$

Where L_1 and L_2 are the self inductances of the primary and the secondary coils respectively (C. M. Zierhofer 1996). The coupling coefficient will equal

1 for perfect coupling between two coils and zero for no interaction.

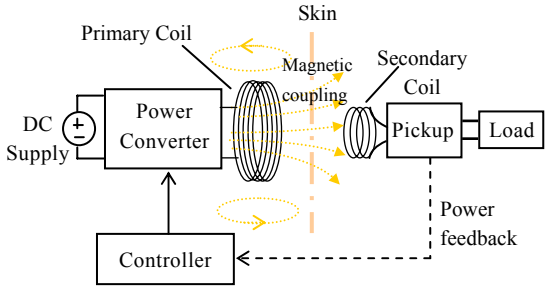

Figure 1: Block diagram of a TET system.

Knowing the coupling coefficient between two coils under a range of orientations is valuable for accessing their ability to transfer sufficient power to the load. This information can be used to guide the design process for primary and secondary coils. The coupling between primary and secondary coils has been categorised into three components:

a) Separation: coils are axially aligned with a separation gap (usually occupied by skin and fat). For an abdominal TET site, this gap is estimated to be within the range of 10 to 30mm.
b) Displacement: where the separation gap between the coils is constant, but their centres are displaced by a distance *x*. Typical range of displacement is estimated to be +/-20mm.
c) Rotation: the primary coil is tilted off-axis with respect to the secondary coil by an angle α.

It is vital to meet the power requirements of the implantable load at various coil orientations, and to not cause excess heating inside the implantable device. Power efficiency is also a valuable element in TET systems as the freedom of the patient is restricted by the weight and duration of the external battery pack they must carry (Hochmair 1984). This paper provides a comparative study of the coupling coefficient and power efficiency of a TET system for various coil coupling conditions.

2 COUPLING ANALYSIS

Three methods of determining the coupling coefficient between primary and secondary coils are presented. The first is an analytical method based on models established by Soma et. al. (Mani Soma 1985). This approach enables calculation of coupling coefficients for a variety of geometrical offsets between two single turn coils. The second method is a finite element approach using JMAG Studio 8.0 to model the coil geometries and numerically solve for the magnetic flux density and coupling coefficient. Finally, physical coils are constructed and the coupling coefficient measured experimentally.

The coil geometry used in the analytical model is considerably simplified in order to provide a tractable closed form solution. This model assumes that the coils are a single turn so that other dimensional data (i.e. internal and external radius) of the coils are ignored. The average radius between the internal and external radius is used in these calculations. The self inductance of L_p and L_s in this instance is taken to be the inductance of a single turn coil. For the simulated model, the coil geometry used is the same as the experimental physical coils.

2.1 Analytical Model

To derive the analytical model, the orientation between the primary and secondary coils needs to be defined. Adopting the same misalignments as used by Soma (Mani Soma 1985), the following three misalignment conditions are considered:

2.1.1 Axially Aligned Separation

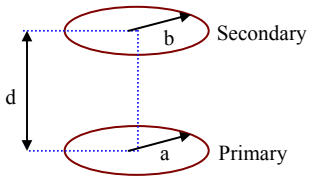

Figure 2: Axially aligned separation.

Figure 2 illustrates the orientation of the coils when they are axially aligned. The distance d represents the minimum separation between the two coils. The characterisation of mutual inductance in this orientation is given by equation 3.

$$M_F = \mu_0 \sqrt{ab} G(s) \tag{3}$$

Where

$$G(s) \equiv \left(\frac{2}{s} - s\right) K(s) - \frac{2}{s} E(s) \tag{4}$$

K(s) refers to the complete elliptic integral of the first kind,

$$K(s) = \int_0^1 [(1-t^2)(1-st^2)]^{-\frac{1}{2}} dt \tag{5}$$

And E(s) is the complete elliptic integral of the second kind,

$$E(s) = \int_0^1 [(1-t^2)^{\frac{1}{2}}(1-st^2)]^{-\frac{1}{2}} dt \quad (6)$$

The variable s, defines the mathematical relationship between the primary and the secondary coils. The formula for s is given by

$$s \equiv \sqrt{\frac{4ab}{(a+b)^2 + d^2}} \quad (7)$$

2.1.2 Lateral Displacement

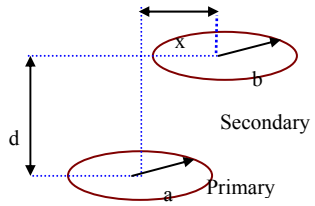

Figure 3: Lateral displacement.

Lateral displacement with parameter x is illustrated in figure 3. Given that x<b in practical situations, the mutual inductance for lateral displacement can be defined by equation 8. G(s) in this equation is also determined by equation (4).

$$M_L = \frac{\mu_0 ab}{\sqrt{a(b+x)}} G(s) \quad (8)$$

Where s becomes

$$s \equiv \sqrt{\frac{4a(b-x)}{(a+b-x)^2 + d^2}} \quad (9)$$

2.1.3 Angular Rotation

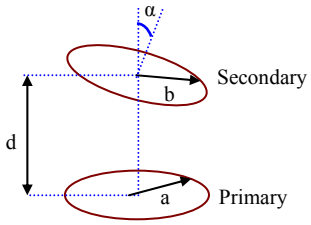

Figure 4: Angular rotation.

Figure 4 demonstrates angular rotation about the z axis. In this analysis, misalignments up to 25° are considered. The value of s used to calculate M_A is taken to be the average value of s_{min} and s_{max}. The formulas used for evaluation of M_A are as follows

$$M_A = \frac{\mu_0 \sqrt{ab}}{\sqrt{\cos a}} G(s_{avg}) \quad (10)$$

Where s_{avg} is

$$s_{avg} = \frac{s_{\min} + s_{\max}}{2} \quad (11)$$

s_{min} and s_{max} are given by

$$s_{\min} \equiv \sqrt{\frac{4ab\cos a}{a^2 + b^2 + d^2 + 2ad\sin a + 2ab\cos a}} \quad (12)$$

$$s_{\max} \equiv \sqrt{\frac{4ab\cos a}{a^2 + b^2 + d^2 - 2ad\sin a + 2ab\cos a}} \quad (13)$$

2.2 Simulated Model

The use of numerical simulation alleviates many of the geometrical simplifications that were used in the previous analytical model. JMAG was used to simulate the coupling relationship between the primary and the secondary coils. Figure 5 illustrates the mesh created for two coils for an axially aligned orientation with 15mm separation. The mesh contained 1435 nodes and 6982 elements. Calculating the magnetic field generated took 6 seconds running on a 3.3GHz PC.

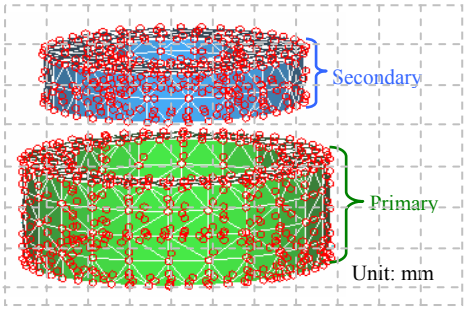

Figure 5: Mesh of primary and secondary coils generated in JMAG – axially aligned.

The coils were defined by the number of turns, physical dimensions, and ESR (Equivalent Series Resistance). Within JMAG, an external circuit was produced to represent the two coils and a sinusoidal current was injected into one of the inflow faces of the primary coil. The secondary coil was shorted to obtain the short circuit current and equation 14 was used to calculate the mutual inductance of the coil for various orientations.

$$M = \frac{I_{sc}}{I_p} L_2 \quad (14)$$

Where I_{sc} is the short circuit rms (Root Mean Square) current in the secondary winding, L_2 is the secondary inductance, and I_p is the primary rms current. Figure 6 shows the magnetic field density contours for a 20mm laterally displaced secondary coil with a separation of 10mm. The magnetic field in the secondary coil is at its highest on the edge facing the primary and gradually drops off to zero on the face furthest from the primary.

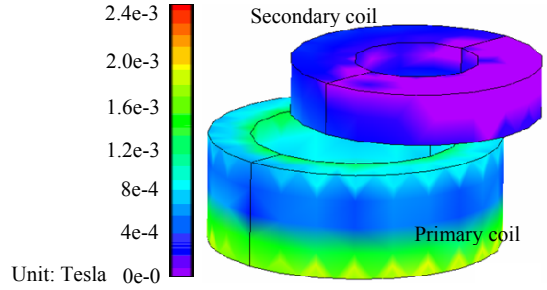

Figure 6: Magnetic field distribution when the secondary coil is laterally displaced by 20mm for a separation of 10mm

2.3 Experimental Measurements

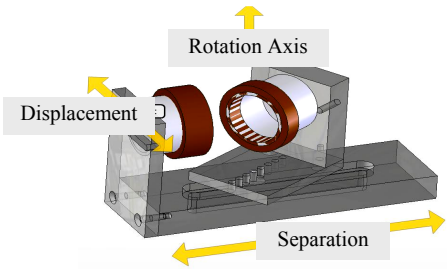

Figure 7: CAD model of physical test rig used to hold primary and secondary coils in known physical orientation.

A test rig was built (see figure 7) to accurately locate the primary and secondary coils at known orientations. The rig allows fixing of the secondary coil in all three misalignments discussed in the previous section. Equation 15 was used for determining the coupling coefficient between the coils.

$$k = \sqrt{1 - \frac{L_{ps\_shorted}}{L_{ps\_open}}} \qquad (15)$$

Where $L_{ps\_shorted}$ is the primary inductance when the secondary is shorted, and L_{ps_open} is the primary inductance when the secondary is open, which is equal to the primary coil inductance L1. At the same time as acquiring coupling coefficient measurements, the efficiency of power transfer was also measured for the whole TET system. The efficiency was computed as the ratio of the power delivered to the medical device over the power drawn from the external battery source supplying the TET system.

3 COUPLING AND EFFICIENCY RESULTS

The first evaluation considered a pair of coils with a very simple geometry which could be accurately represented using all methods. Both coils used a single winding and figure 8 illustrates the effect on the coupling coefficient when the lateral displacement is increased from 0 to 20 mm at 10mm separation. The lines ka, ks and kp corresponds to the coefficient of coupling from the analytical model, simulated model and experimental measurements respectively. As expected the coupling coefficient drops as the lateral displacement increases, and all three methods produced consistent results. Similar consistency is seen for axial alignment and angular rotation cases.

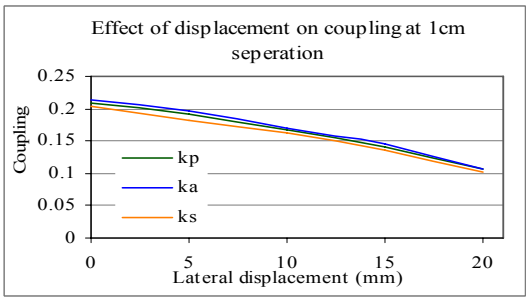

Figure 8: The effect of lateral displacement on coupling at 10mm separation.

However, practical TET coils will not consist of single turns, and they will have bulk which can be characterised by internal and external radius and also a physical height. Physical coils were constructed with a self inductance of 30.4µH for the primary and 8.75µH for the secondary coil.

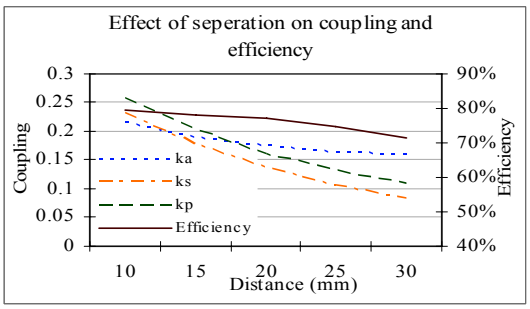

Figure 9: Effects of separation between coils on coupling and efficiency when the coils aligned axially.

The three methods of evaluating the coupling coefficient were implemented using genuine physical parameters, and the results are shown in figure 9. With the coils aligned axially, the coupling coefficient decreases as the separation increases. The simulated coupling coefficients have a mean deviation of 16% from the experimental results. However, the analytical results are far away. This is illustrating the effects of the physical bulk of the coils. The efficiency of the power transfer is also shown in figure 9. The coupling coefficient drops at a greater rate than the efficiency. This is illustrating that, although the coupling coefficient may be low, good power efficiency can still be achieved.

Figure 10 illustrates the effects of displacement on coupling and efficiency when the coils are separated by 10mm and 20mm. Again, the simulated and practical coupling coefficients are fairly similar (with a mean deviation of 9.5%), while the analytical model significantly under estimates the practical result at 10mm separation. However at 20mm separation, the analytical coupling coefficient is in much better agreement with the simulated results. This suggests that for lateral displacement at larger separations, the magnetic coupling for the physical coils is reasonably well represented by idealised coils. The effect of lateral displacement on efficiency was very small (efficiency dropped from 79% to 77% for 20mm lateral displacement) at 10mm separation. Efficiency drops more rapidly down to 72% at 20mm separation.

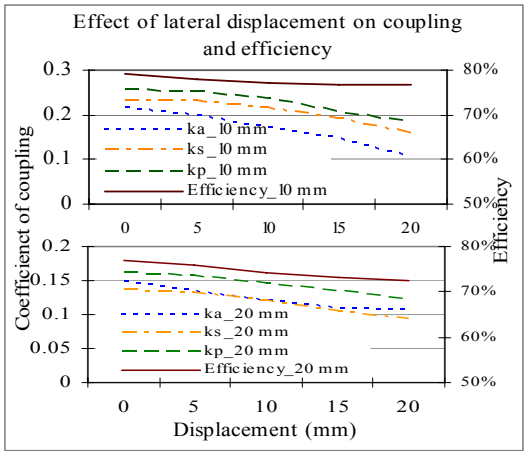

Figure 10: Effects of displacement on coupling and efficiency for coil separations of 10mm and 20mm.

The impact of rotational misalignment on coupling was similar to the lateral displacement case. The simulation result underestimated the practical coupling for both 10mm and 20mm separation however it was within a mean deviation of 14.76% of the experimental measurements.

4 DISCUSSION

The maximum power transfer of a TET system refers to the maximum power that can be transferred from primary to secondary coil disregarding the losses associated with the components in the circuit. The maximum power that can be transferred by a current-fed push-pull resonant converter TET system has been derived by Si et. al. (Ping Si 2007) using mutual inductance between the primary and secondary coils. This relationship is shown in equation 16 as a function of the coupling coefficient.

$$P_{\max} = \frac{\pi k V_{dc}}{8 f \sqrt{L_p L_s}} V_{in} \qquad (16)$$

Where L_p and L_s are the primary and secondary coil inductances, k is the coupling coefficient, P_{max} is the maximum power transfer, V_{in} is the DC input voltage, V_{dc} is the output voltage at the load and f is the system resonant operating frequency.

Equation 16 is based on the assumption that high order harmonic components are negligible and the dc current is continuous at the pickup. These assumptions are reasonable for practical circuits. Equation 16 shows that for given primary and secondary circuits, the maximum power transfer capacity of a TET system is proportional to the coupling coefficient. Good coupling can increase the maximum possible power transfer from primary to secondary coils. However, in terms of the power efficiency, from the previous results shown in section 3, it is clear that coupling does not have a dramatic effect. This is a very important feature of the system, meaning it is possible to achieve high power efficiency for a loosely coupled TET system.

During the power transfer process, there is little power loss in the air gap between the primary and the second coils. Therefore the coupling coefficient is not sensitive to the overall power efficiency of the system. However with low coupling, high magnetic strength is required to deliver the same amount of power, so the required current and/or voltage use to generate the field needs to be higher, resulting in a higher loss in the drive circuits. To further understand the power efficiency issue, the power losses in each component of the TET system was identified.

The loss components were measured from the TET system and are presented in figure 11. The total power loss between the input and output of the system was also measured, and the difference

between the sum of the identified primary and secondary losses, and the actual total losses measured are presented as "Other" in figure 11. The experiment was conducted under a constant load of 10W, and the input power to the TET system was adjusted accordingly for each alignment configuration to maintain the output power to be constant.

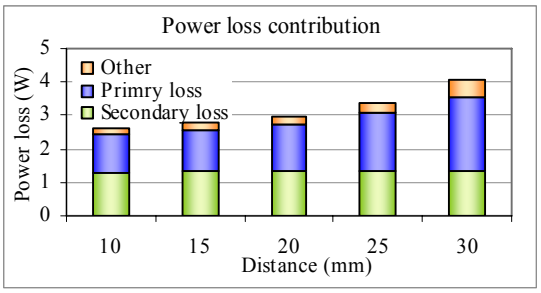

Figure 11: Loss contributions for fully aligned case when delivering 10W to a load.

Figure 11 shows that the total power loss increases when the separation between the coils is larger. However the power loss at the secondary power circuit is more or less the same due to the same load and circuit operating condition. This means no additional losses are occurring at the secondary even when the coupling is poorer. Thus there is no complication of temperature rise and risk of tissue damage.

The increase in total system loss is mainly from the primary power circuit due to the need for higher coil currents to compensate when the air gap separation is larger. A higher strength magnetic field is needed thus the current in the primary coil and its tuning capacitor has to be higher, resulting in higher losses. In this circuit losses in other parts of the primary converter such as dc conduction losses and switching losses also increase at the same time due to the increased dc voltage at the input. However, they are relatively small because the dc current of the primary converter is relatively small compared to the ac resonant current. Therefore (Equivalent Series Resistance) ESR values for the primary coil and tuning capacitor are important parameters to consider in designing an efficient TET system.

5 CONCLUSIONS

Three methods of determining the coupling coefficient for specific coil orientations covering the typical range of TET coils suitable for supplying 10W of power are presented in this paper. The analytical method was shown to be valid for idealised coil configurations although it could not be used to model the actual experimental setup accurately. Numerical simulation gave a superior match with experimental results, and is appropriate for assessing different coil designs efficiently.

The coupling coefficient is a major factor determining the maximum power transfer capacity of a TET system. However, it does not determine the system power efficiency. Power losses at the implant were shown to be largely constant. Therefore there is no additional heat and temperature rise when the coupling becomes poorer. A small overall power efficiency drop was caused mainly by the ESR losses in the primary circuit. With a maximum coil separation of 30mm, the variation in coupling coefficient reduced the overall power efficiency from approximately 80% to 70%.

REFERENCES

C. M. Zierhofer, E. S. H. (1996). "Geometric approach for coupling enhancement of magnetically coupled coils." IEEE transactions on biomedical engineering 43: 708-714.

F.C Flack, E. D. J., D. M. Schlapp (1971). "Mutual inductance of air-cored coils: Effects on design of radio-frequency coupled implants." Medical and Biological Engineering 9: 79-85.

Hochmair, E. S. (1984). "System optimization for improved accuracy in transcutaneous signal and power transmission." IEEE transactions on biomedical engineering 31: 177-186.

John C. Schuder, J. H. G., Hugh E. Stephenson Jr (1971). "An inductively coupled RF system for the transmission of 1kW of power through the skin." IEEE transactions on biomedical engineering 18: 265-273.

Mani Soma, D. C. G., Robert L. White (1985). "Radio-frequency coils in implantable devices: Misalignment analysis and design procedure." IEEE transactions on biomedical engineering 34: 276-282.

N. de N. Donaldson, T. A. P. (1983). "Analysis of resonant coupled coils in the design of radio frequency transcutaneous links." Medical and Biological Engineering and computing 21: 612-627.

Ping Si, P. A. H., J. W. Hsu, M. Chiang, Y. Wang, Simon Malpas, David Budgett (2007). "Wireless power supply for implantable biomedical device based on primary input voltage reglation." 2nd IEEE conference on Industrial Electronics and Applications.